JOURNAL OF GUIDANCE, CONTROL, AND DYNAMICS
Vol. 28, No. 1, January–February 2005

Engineering Notes

ENGINEERING NOTES are short manuscripts describing new developments or important results of a preliminary nature. These Notes cannot exceed 6 manuscript pages and 3 figures; a page of text may be substituted for a figure and vice versa. After informal review by the editors, they may be published within a few months of the date of receipt. Style requirements are the same as for regular contributions (*see inside back cover*).

Precision Positioning of a Parallel Manipulator for Spacecraft Thrust Vector Control

Kougen Ma* and Mehrdad N. Ghasemi-Nejhad†
University of Hawaii at Manoa, Honolulu, Hawaii 96822

Introduction

BECAUSE the ability to control the thrust vector of any propulsion system is extremely advantageous, thrust vector control (TVC) has been considered a key area of research in launch systems, upper stages, and vertical or short takeoff, vertical landing aircraft. For example, a thrust vector controller for a space shuttle vehicle with multiple engines was presented by Redmill et al.[1] This controller maintained vehicle trajectory and thrust vector while minimizing risk and damage to each engine and to the propulsion system as a whole by independently controlling the thrust magnitude and exhaust cone gimbal angles of each engine. For rockets, missiles[2] and jet planes,[3,4] TVC becomes a crucial technology for controlling their trajectories and achieving high maneuverability. In satellite systems, TVC can be used to correct the misalignment caused by the thruster firing and the shift of the mass center of a satellite due to fuel consumed, solar panels deployed, onboard experiments carried out, etc.

The thrust vector of a satellite thruster should ideally pass through the mass center of the satellite; however, it practically does not, which induces a so-called thrust vector misalignment. Thrust vector misalignment results in a disturbance torque that causes satellite rotation, long orbit-transfer time, extra requirements of attitude/orbit control systems, and large positioning error. To eliminate the effect of thrust vector misalignment, reaction control subsystem (RCS) thrusters, which are additional to the main thruster, are conventionally used in satellites. However, RCS thrusters obviously consume additional satellite fuel, thus, shortening the satellite life. Moreover, the firing of the main thruster in a satellite generates vibration that resonates throughout satellite structure. In addition to the RCS thrusters, using a steerable main thruster is another alternative for TVC of satellites; nevertheless, many issues related to using a steerable main thruster are still open, such as how to steer the thruster, how to make the steering mechanism as light as possible, and how to control the steering mechanism.

The emerging intelligent composite structures technology provides a promising technical venue toward TVC of satellites. Hexapod Stewart platforms with six degrees of freedom for the top device plate (see Refs. 5–9) have been developed for precision positioning or vibration suppression as optical benches, although some of them may not possess considerable motion ranges or frequency bands. In the Intelligent and Composite Materials Laboratory of the University of Hawaii at Manoa (UHM), an intelligent composite platform[10] or parallel manipulator is being developed. The UHM parallel manipulator incorporates composites, sensors, actuators, and controllers as a means for fine-tuning position tolerances during thruster firing and possesses simultaneous precision positioning and vibration suppression capabilities to provide two in-plane rotational degrees of freedom for the top device plate.

In terms of control strategies of platforms, the controller designs for most of the Hexapod Stewart platforms are based on traditional control theory, with a separated control loop closed around each strut, that is, the single-input/single-output (SISO) approach. Because of the cross communications among the struts, the system is not, in practice, SISO. Therefore, a comprehensive study on control strategies of such parallel manipulators is necessary.

This Note presents the inverse kinematics, singularity analysis, control strategies, and experiments for the UHM parallel manipulator with the TVC application. First, the general configuration of the UHM intelligent parallel manipulator is introduced. Next, the kinematics and singularity analysis of the parallel manipulator are conducted. An intelligent control approach for the precision positioning is then presented, and two control strategies, namely, local control strategy and global control strategy, are proposed. Finally, the experiments and comparisons are performed, followed by discussions and conclusions.

UHM Composite Precision Parallel Manipulator

Figure 1 shows the UHM intelligent parallel manipulator with two degrees of tip-tilt freedom and its application to the TVC of a satellite. This parallel manipulator consists of a lower composite base, a top circular composite device plate, three active composite struts, and a central support. The three active struts are connected to the vertices of the base and the top device plate through joints. The top device plate is constrained to pivot about the central joint of the central support as the active struts extend or retract. This feature allows not only precision control of the angular displacement of the top device plate but also the thrust transmission of an axial thruster mounted on the top device plate. Each strut consists of a large-stroke dc motor with an encoder and a piezoelectric stack actuator. The dc motor has high resolution with low-power consumption, which is excellent for precision positioning. Its maximum stroke, maximum velocity, unidirectional repeatability, maximum input voltage, and minimum incremental motion are 50 mm, 1 mm/s, 0.1 μm, 12 V, and 0.05 μm, respectively. Its maximum push/pull force is about 100 N. The incremental encoder with resolution of 2048 counts per revolution is mounted on each motor shaft to measure the displacement/velocity of each strut. To achieve the vibration control beyond the frequency bandwidth of the motor, a piezoelectric stack actuator (PZT-5A) is integrated in each strut, due to the PZT-5A high-frequency bandwidth. The preload, maximum load, resolution, maximum stroke, and maximum input voltage of the piezoelectric stack actuator are 150 N, 1000 N, 0.02 μm, 20 μm, and 150 V, respectively. The geometry of the manipulator is optimized to guarantee the required motion range of the top device plate and the major thrust transmission through the central support.

Received 25 May 2004; revision received 8 September 2004; accepted for publication 8 September 2004.

*Assistant Researcher, Intelligent and Composite Materials Laboratory, Department of Mechanical Engineering.

†Professor, Intelligent and Composite Materials Laboratory, Department of Mechanical Engineering.

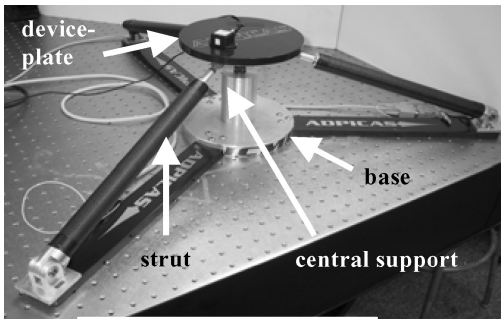

a) Manipulator

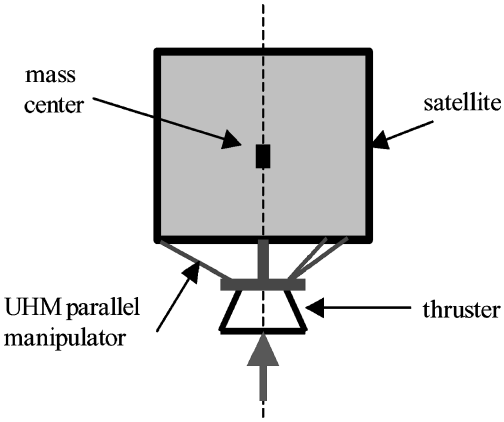

b) Satellite TVC

Fig. 1 UHM two-degree-of-freedom intelligent parallel manipulator and satellite TVC application.

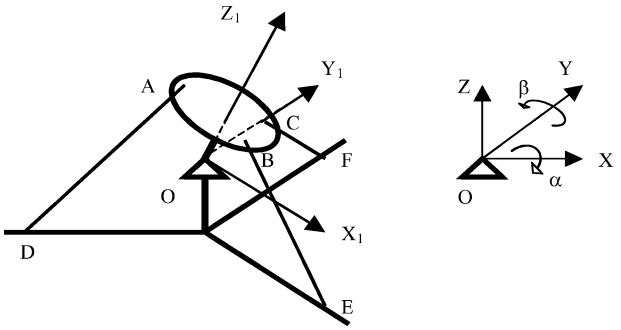

Fig. 2 Coordinate systems.

In the TVC of a satellite (Fig. 1b), the UHM intelligent parallel manipulator is located between the satellite and its main thruster. The base of the parallel manipulator is connected to the satellite structure, and the main thruster is mounted onto the top device plate. By the control of the motion of the struts of the parallel manipulator, the thrust vector misalignment can be corrected, that is, the thrust vector of the main thruster always passes through the mass center of the satellite, thus, eliminating unexpected rotations of the satellite.

Inverse Kinematics and Singularity Analysis

Figure 2 shows the schematic of the UHM parallel manipulator, where A, B, and C in the top device plate are the joining points between the top device plate and the three active struts; D, E, and F in the base are joining points between the base and the struts; and O is a pivot around which the top device plate can tilt. To derive the inverse kinematics, two coordinate systems are assumed: XYZO and $X_1Y_1Z_1O$. XYZO is fixed to the base at O, and $X_1Y_1Z_1O$ is fixed to the top device plate at O and movable relative to the base. The tilt angles around the OX and OY axes are defined as α and β, respectively.

Following the procedure presented by Ma and Ghasemi-Nejhad,[11] the length change (motion) of each strut can be obtained as

$$\Delta L_{AD} = L_{AD} - L^0_{AD}, \qquad \Delta L_{BE} = L_{BE} - L^0_{BE}$$
$$\Delta L_{CF} = L_{CF} - L^0_{CF} \tag{1}$$

where ΔL_{AD}, ΔL_{BE}, and ΔL_{CF} are the changes of lengths of L_{AD}, L_{BE}, and L_{CF} at the tilt angles α and β relative to their initial lengths L^0_{AD}, L^0_{BE}, and L^0_{CF}, respectively,

$$L^2_{AD} = R^2 + r^2 + h_1^2 + h_2^2 - 2Rr\cos\beta + 2rh_2\sin\beta + 2h_1\cos\alpha(R\sin\beta + h_2\cos\beta) \tag{2}$$

$$L^2_{BE} = R^2 + r^2 + h_1^2 + h_2^2 - rh_2\left(\sin\beta + \sqrt{3}\sin\alpha\cos\beta\right) - 0.5Rr\left(3\cos\alpha + \cos\beta - \sqrt{3}\sin\alpha\sin\beta\right) - h_1R\left(\sqrt{3}\sin\alpha + \cos\alpha\sin\beta\right) + 2h_1h_2\cos\alpha\cos\beta \tag{3}$$

$$L^2_{CF} = R^2 + r^2 + h_1^2 + h_2^2 - rh_2\left(\sin\beta - \sqrt{3}\sin\alpha\cos\beta\right) - 0.5Rr\left(3\cos\alpha + \cos\beta + \sqrt{3}\sin\alpha\sin\beta\right) + h_1R\left(\sqrt{3}\sin\alpha - \cos\alpha\sin\beta\right) + 2h_1h_2\cos\alpha\cos\beta \tag{4}$$

$$L^0_{AD} = L^0_{BE} = L^0_{CF} = \sqrt{(R-r)^2 + (h_1+h_2)^2} \tag{5}$$

where R and r are the effective radii of the base and the top device plate, respectively, and h_1 and h_2 are the distances from the pivot to the center of the top device plate and to the center of the base, respectively. For the UHM parallel manipulator, $R = 440$ mm, $r = 72.5$ mm, $h_1 = 23$ mm, and $h_2 = 100$ mm. Inverse kinematics demonstrates that the struts motion is about 1 mm for tilting the top device plate by 1 deg around the OX and OY axes.

According to Eq. (1), the relationship between the tilt angular velocities and the strut velocities is as follows:

$$\begin{Bmatrix} \Delta\dot{L}_{AD} \\ \Delta\dot{L}_{BE} \\ \Delta\dot{L}_{CF} \end{Bmatrix} = \begin{bmatrix} J^{\alpha}_{AD}(\alpha,\beta) & J^{\beta}_{AD}(\alpha,\beta) \\ J^{\alpha}_{BE}(\alpha,\beta) & J^{\beta}_{BE}(\alpha,\beta) \\ J^{\alpha}_{CF}(\alpha,\beta) & J^{\beta}_{CF}(\alpha,\beta) \end{bmatrix} \begin{Bmatrix} \dot{\alpha} \\ \dot{\beta} \end{Bmatrix} = J \begin{Bmatrix} \dot{\alpha} \\ \dot{\beta} \end{Bmatrix} \tag{6}$$

where $\Delta\dot{L}_{AD}$, $\Delta\dot{L}_{BE}$, and $\Delta\dot{L}_{CF}$ are the velocities of the three struts; $\dot{\alpha}$ and $\dot{\beta}$ are the tilt angular velocities of the top device plate about OX and OY axes, respectively; $J^{\alpha}_{AD}(\alpha,\beta), \ldots, J^{\beta}_{CF}(\alpha,\beta)$ are the sensitivity functions of the length changes of the three struts with respect to the tilt angles α or β, that is, $J^{\alpha}_{AD}(\alpha,\beta) = \partial\Delta L_{AD}/\partial\alpha$, $J^{\beta}_{AD}(\alpha,\beta) = \partial\Delta L_{AD}/\partial\beta$, etc.; and J is the Jacobian matrix.

Because of the overconstrained feature of the parallel manipulator, the three struts have to be controlled carefully to avoid kinematic singularity. The possible struts configurations include replacing one of the three struts with a dummy strut or controlling two of them in tandem. Either of these two configurations results in nonzero eigenvalues for the Jacobian matrix given in Eq. (6), indicating that singularity does not exist in these two configurations.

Control Strategies, Experiments, and Comparisons

Based on the architecture of the parallel manipulator, two control strategies, namely, local control strategy (LCS) and global control strategy (GCS), are proposed and experimentally verified. The experimental control system consists of a data acquisition and control computer, amplifiers for the struts, the UHM parallel manipulator, a tilt sensor, and signal analyzers. The data acquisition and control system includes two processor boards, a 32-channel A/D board, a 32-channel D/A board, and a decoder board for decoding the signal from the integrated encoder in each strut. The controllers are programmed in MATLAB® simulink[12] and then downloaded to the

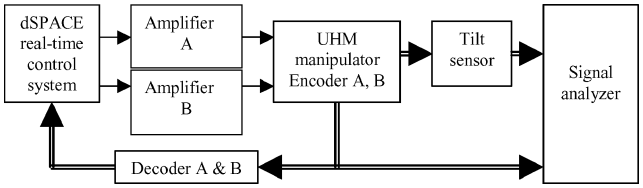

Fig. 3 LCS schematic.

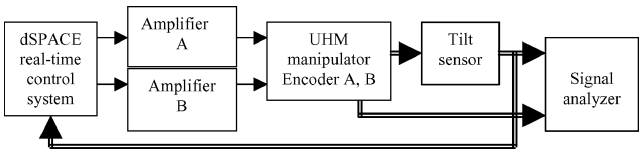

Fig. 4 GCS schematic.

data acquisition and control computer. In addition, only two struts of the parallel manipulator are controlled, and the third one is replaced with an air damper to simplify the experiments.

Figure 3 is a schematic of the LCS experiment in which each active composite strut is controlled individually. The displacement of each strut is measured by employing the integrated encoder, and this displacement is fed back to each strut motion input end. Obviously, a mapping from the desired tilt angles to the motion commands of the struts is needed to find out the required motion of the struts for given tilt angles. This mapping can be obtained by the following methods: 1) inverse kinematics analysis, 2) inverse kinematics modeling using advanced technologies such as neural network, and 3) experimental kinematics measurements. In this work, the third technique is used to account for nonlinearities in the joints and struts. The tilt angle accuracy of this control strategy depends on the understanding of the parallel manipulator kinematics because no tilt angle information is used for this control strategy directly. Although a tilt sensor is included in Fig. 3, note that this tilt sensor is used for monitoring purpose only and is not included in the control loops.

Figure 4 is a schematic of the GCS experiment in which the tilt senor on the top device plate is used to measure the tilt of the top device plate where the thruster is mounted in the TVC application of satellites. The tilt angle signals are fed back to the global controller. The tilt angle errors become the inputs of the global controller. This control strategy has many advantages. For example, the tilt angle accuracy is controlled directly, no kinematics information is required, and the effects of the nonlinearities of joints and struts are accounted for by the controller.

Fuzzy logic control (FLC)[12–14] is chosen in both the LCS and GCS. The FLC is capable of providing the high degree of accuracy required by high-performance linear or nonlinear systems, without the need of detailed system mathematical models. Therefore, the FLC is an appropriate control technique for the UHM parallel manipulator due to the existing nonlinearities in the joints and struts and the kinematics nonlinearities of the manipulator.

The FLC uses a form of quantification of imprecise information, that is, input fuzzy sets, to generate an inference scheme, which is based on a knowledge base of control signals to be applied to the system. A FLC comprises four primary components: 1) fuzzifier (the values of the state variables monitored during the process fuzzified into fuzzy linguistic terms), 2) knowledge base that contains fuzzy IF–THEN rules and membership functions, 3) fuzzy reasoning (which results in a fuzzy output for each rule), and 4) defuzzification interface. In the following experiments, the strut position errors in the LCS and the tilt angle errors in the GCS are used as the input variables. In both control strategies, seven input fuzzy sets are defined for the input variables and five output fuzzy sets for the output variables. The seven input fuzzy sets are negative large (NL), negative medium (NM), negative small (NS), zero (Z), positive small (PS), positive medium (PM), and positive large (PL), and the five output fuzzy sets are NL, NS, Z, PS, and PL. In addition, the centroid method is used to defuzzify outputs into crisp values. The membership functions of the input and output variables of the FLCs are Gaussian-shaped functions, where the defined varying ranges are $[-2, 2]$ for all input variables and $[-10, 10]$ for all output variables. The inference scheme employed is as the following:

IF (input is (NL or NM)) THEN (output is NL);

IF (input is NS) THEN (output is NS);

IF (input is Z) THEN (output is Z);

IF (input is PS) THEN (output is PS);

and

IF (input is (PL or PM)) THEN (output is PL).

Figure 5 shows the desired tilt angles of the top device plate, which are in square wave with amplitude of 1 deg and frequency of 0.05 Hz, the actual tilt angles, as well as the tilt angle errors for the LCS and GCS. The steady-state errors of α are 0.022 deg, that is, relative error is 2.2% because the command is 1 deg, in the positive tilt angle and 0.044 deg, that is, 4.4%, in the negative tilt angle for the LCS, and these values decrease to 0.003 deg, that is, 0.3%, and 0.015 deg, that is, 1.5%, for the GCS. Similarly, the steady-state errors of β are 0.007 deg, that is, 0.7%, in the positive tilt angle and 0.035 deg, that is, 3.5%, in the negative tilt angle for the LCS and 0.007 deg, that is, 0.7%, and 0.009 deg, that is, 0.9%, for the GCS. The average steady-state relative errors of α and β are 3.3 and 2.1% for the LCS and 0.9 and 0.8% for the GCS, respectively. The settling times with a 2% relative error tolerance are greater than 10 s for the LCS. For the GCS, the settling times are about 4 s for α and 4.5 s for β with the same 2% relative error tolerance.

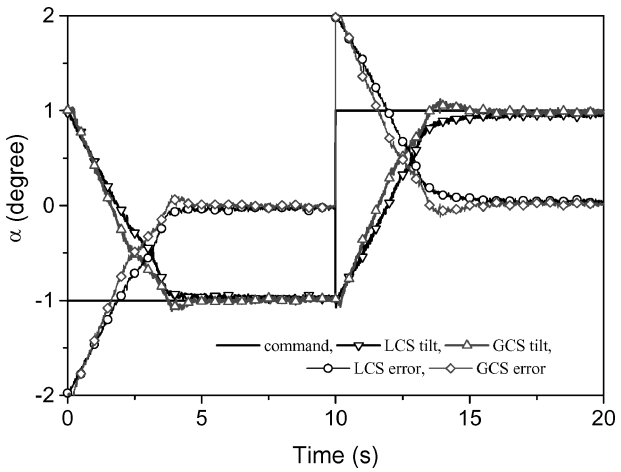

a) α

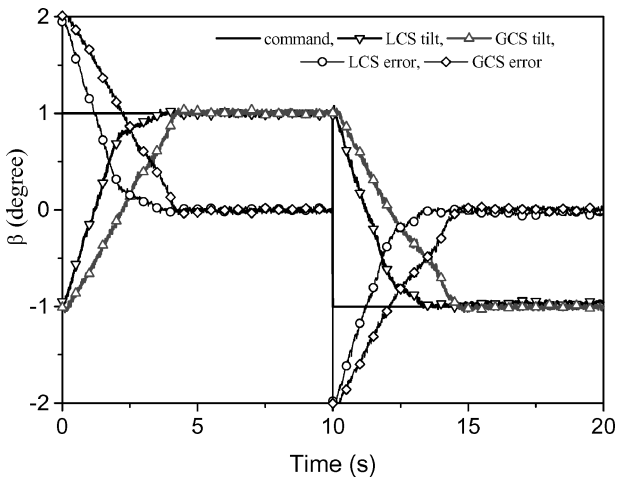

b) β

Fig. 5 Commands, tilt angles, and errors.

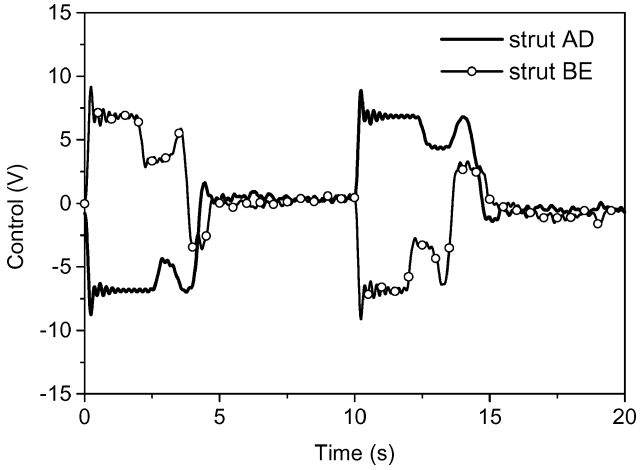

Fig. 6 Control signal (GCS).

The experiments also show that the struts AD and BE have to move 0.8 and 1.5 mm, respectively, to achieve the tilt angles of $\alpha = \beta = \pm 1$ deg. These strut motions are consistent with the inverse kinematics analysis.

The experimental results reveal that the LCS delivers lower positioning accuracy compared with the GCS, especially for α. The following sensitivity analysis can help better understand this feature. The inverse sensitivities of the strut motions over α and β can be obtained by calculating the partial derivatives of the strut motions in Eq. (1) with respect to α and β, that is, $J^{\alpha}_{AD}(\alpha, \beta)$, $J^{\alpha}_{BE}(\alpha, \beta)$, $J^{\beta}_{AD}(\alpha, \beta)$, and $J^{\beta}_{BE}(\alpha, \beta)$ in Eq. (6). The results imply that $J^{\alpha}_{AD}(\alpha, \beta)$, $J^{\alpha}_{BE}(\alpha, \beta)$, $J^{\beta}_{AD}(\alpha, \beta)$, and $J^{\beta}_{BE}(\alpha, \beta)$ vary in the ranges of $[-0.002, 0.002]$, $[-0.703, -0.65]$, $[0.76, 0.803]$, and $[-0.43, -0.375]$ mm/deg, respectively, whereas the tilt angles α and β change in the range of $[-1, 1]$ deg. This means that the reciprocals of these inverse sensitivities are in the ranges of $[-500, 500]$, $[-1.422, -1.538]$, $[1.316, 1.245]$, and $[-2.326, -2.667]$ deg/mm, respectively. On the average, the last three, that is, $1/J^{\alpha}_{BE}(\alpha, \beta)$, $1/J^{\beta}_{AD}(\alpha, \beta)$, and $1/J^{\beta}_{BE}(\alpha, \beta)$, are about -1.48, 1.281, and -2.497 deg/mm, respectively, in the given ranges of α and β, but the first one, that is, $1/J^{\alpha}_{AD}(\alpha, \beta)$, is much greater, implying that a small change in the length of the strut AD will produce a large tilt angle change of α. As mentioned earlier, each strut motion in the LCS approach is directly measured and individually controlled. Inevitably, the existing tolerances of the joints and motors cannot, therefore, be accounted for and, hence, compensated in the LCS and cause positioning error of the entire parallel manipulator.

Figure 6 shows the control signals for the GCS, demonstrating the unique characteristics of the designed FLC as stated in the following. First, the control signal is large, that is, the struts move fast, when the error is large to reduce rapidly the error. Second, as the error becomes smaller, the control signal becomes smaller as well. Third, when the control signal becomes so small that it cannot drive the strut any longer due to the existing friction in the strut, the control signal is raised so that the strut can still move to decrease the position error. Finally, the control signal is zero when the error is zero. This unique characteristic of the controller makes the position accuracy of an arc-minute available in the GCS.

Conclusions

This investigation verifies that the use of the two-degree-of-freedom UHM intelligent parallel manipulator, with integrated smart and composite structures technology, for the TVC of satellites is feasible. When the control configuration is properly organized, the kinematic singularity does not exist. FLC is a suitable control method for the UHM parallel manipulator because FLC is model-free and is easy to handle systems nonlinear characteristics such as backlash and friction in the struts and joints as well as the inherent kinematics nonlinearities of the parallel manipulator. The experiments imply that both the LCS and GCS can work well and the GCS can provide smaller steady-state errors and shorter settling time. The LCS is more sensitive to the existing uncertain change of the strut lengths due to the gaps in the joints and motors that are hardly accounted for in the LCS.

Future studies will be simulations and experiments in a larger spectrum to test the TVC of a satellite, which includes the UHM intelligent parallel manipulator control as reported in this Note, a satellite dynamic model, and a satellite attitude controller.

Acknowledgments

The authors acknowledge the financial support of the Office of Naval Research for the Adaptive Damping and Positioning using Intelligent Composite Active Structures Project under Grant N00014-00-1- 0692 with Kam W. Ng serving as Program Officer.

References

[1]Redmill, K., Ozguner, U., Musgrave, J., and Merrill, W., "Intelligent Hierarchical Thrust Vector Control for a Space Shuttle," *IEEE Control Systems Magazine*, Vol. 4, No. 3, 1994, pp. 13–23.

[2]Yeh, F. K., Cheng, K., and Fu, L., "Variable Structure Based Nonlinear Missile Guidance and Autopilot Design for a Direct Hit with Thrust Vector Control," *Proceedings of the 41st IEEE Conference on Decision and Control*, IEEE Publications, Piscataway, NJ, 2002, pp. 1275–1280.

[3]Van der Veer, M. R., and Strykowski, P. J., "Counterflow Thrust Vector Control of Subsonic Jets: Continuous and Bistable Regimes," *Journal of Propulsion and Power*, Vol. 13, No. 3, 1997, pp. 412–420.

[4]Bosworth, J. T., and Stoliker, P. C., "The X-31A Quasi-Tailless Flight Test Results," NASA TP 3624, June 1996.

[5]Anderson, E. H., Moore, D. M., and Fanson, J. L., "Development of an Active Truss Element for Control of Precision Structures," *Optical Engineering*, Vol. 29, No. 11, 1990, pp. 1333–1341.

[6]Li, X., Hamann, J. C., and McInroy, J. E., "Simultaneous Vibration Isolation and Positioning Control of Flexure Jointed Hexapods," *Proceedings of SPIE Conference on Smart Structures and Integrated Systems*, Vol. 4327, Society of Photo-Optical Instrumentation Engineers, Bellingham, WA, 2001, pp. 99–109.

[7]McInroy, J. E., and Jafari, F., "The State-of-the-Art and Open Problems in Stabilizing Platforms for Pointing and Tracking," *Proceedings of SPIE Conference on Smart Structures and Integrated Systems*, Vol. 4701, Society of Photo-Optical Instrumentation Engineers, Bellingham, WA, 2002, pp. 177–188.

[8]*Micropositioning, Nanopositioning, Nanoautomation*, Physik Instrumente (PI), GmbH and Co., Karlsruhe, Germany, 2001, pp. 7–16.

[9]Stewart, D., "A Platform with Six Degrees of Freedom," *Proceedings of Institute of Mechanical Engineers*, Vol. 180, No. 15, 1965, pp. 371–386.

[10]Ghasemi-Nejhad, M. N., and Doherty, K. M., "Modified Stewart Platform for Spacecraft Thruster Vector Control," Proceedings of ASME International Mechanical Engineering Congress and Exposition, American Society of Mechanical Engineers, Paper IMECE2002-39032, 2002.

[11]Ma, K., and Ghasemi-Nejhad, M. N., "Two-DOF Precision Platform for Spacecraft Thrust Vector Control: Control Strategies and Simulations," *Proceedings of SPIE Conference on Smart Structures and Integrated Systems*, Vol. 5390, Society of Photo-Optical Instrumentation Engineers, Bellingham, WA, 2004, pp. 46–57.

[12]*Fuzzy Logic Toolbox*, MathWorks, Natick, MA, 2001.

[13]Ma, K., and Ghasemi-Nejhad, M. N., "Simultaneous Precision Positioning and Vibration Suppression of Flexible Manipulators," *Proceedings of the 1st Workshop on Advanced Smart Materials and Smart Structures Technology*, DEStech Publications, Lancaster, PA, 2004, pp. 636–643.

[14]Verbruggen, H. B., and Babuška, R., *Fuzzy Logic Control: Advances in Applications*, World Scientific, Singapore, 1999.